Cell

Transient Non-native Hydrogen Bonds Promote Activation of a Signaling Protein

Alexandra K. Gardino,[1,2,3] Janice Villali,[1,2] Aleksandr Kivenson,[1] Ming Lei,[1] Ce Feng Liu,[1] Phillip Steindel,[1] Elan Z. Eisenmesser,[1,4] Wladimir Labeikovsky,[1,5] Magnus Wolf-Watz,[1,6] Michael W. Clarkson,[1] and Dorothee Kern[1,*]
[1]Department of Biochemistry and Howard Hughes Medical Institute, Brandeis University, Waltham, MA 02452, USA
[2]These authors contributed equally to this work
[3]Present address: David H. Koch Institute for Integrative Cancer Research, MIT, Cambridge, MA 02139, USA
[4]Present address: School of Medicine, University of Colorado, Denver, CO 80204, USA
[5]Present address: Laboratory of Cardiac/Membrane Physiology, Rockefeller University, New York, NY 10065-7919, USA
[6]Present address: Department of Chemistry, University of Umeå, Umeå SE-901 87, Sweden
*Correspondence: dkern@brandeis.edu
DOI 10.1016/j.cell.2009.11.022

SUMMARY

Phosphorylation is a common mechanism for activating proteins within signaling pathways. Yet, the molecular transitions between the inactive and active conformational states are poorly understood. Here we quantitatively characterize the free-energy landscape of activation of a signaling protein, nitrogen regulatory protein C (NtrC), by connecting functional protein dynamics of phosphorylation-dependent activation to protein folding and show that only a rarely populated, pre-existing active conformation is energetically stabilized by phosphorylation. Using nuclear magnetic resonance (NMR) dynamics, we test an atomic scale pathway for the complex conformational transition, inferred from molecular dynamics simulations (Lei et al., 2009). The data show that the loss of native stabilizing contacts during activation is compensated by non-native transient atomic interactions during the transition. The results unravel atomistic details of native-state protein energy landscapes by expanding the knowledge about ground states to transition landscapes.

INTRODUCTION

Proceeding from the original description of an energy landscape for a folded protein, based on classical experiments on myoglobin by Frauenfelder and coworkers (Austin et al., 1975; Frauenfelder et al., 1991), this concept has been applied to protein folding, expanding the conformational space from the native to the unfolded states (Dill and Chan, 1997; Dobson et al., 1998; Vendruscolo and Dobson, 2005; Wolynes, 2005). While the energy landscape idea is widely accepted for folding, it has only recently been embraced for protein function within the native state. Specifically, the existence of discrete conformational substates and resulting shifts of populations by binding of ligands, originally proposed for multisubunit proteins (Monod et al., 1965), are likely to be a general paradigm for protein function (Boehr et al., 2006a, 2006b; Henzler-Wildman and Kern, 2007; Kumar et al., 2000; Li et al., 2008; Mulder et al., 2001; Tsai et al., 2009; Lau and Roux, 2007; Ravindranathan et al., 2005; Yang et al., 2009).

This concept was proposed for the single-domain signaling domain of nitrogen regulatory protein C ($NtrC^r$) where nuclear magnetic resonance (NMR) analysis described a population shift between an inactive and active substate by phosphorylation or activating mutations (Volkman et al., 2001). NtrC, a transcriptional activator, belongs to the family of "two-component systems," the prototypical switch proteins in bacterial signaling (Stock and Guhaniyogi, 2006; Stock et al., 2000). The inactive to active conformational switch of the N-terminal domain ($NtrC^r$) resulting from phosphorylation of D54 involves an extensive change in structure (Figure 1A) (Kern et al., 1999). Activation through a shift in a pre-existing equilibrium between the inactive and active conformation rather than an induced fit mechanism has been proposed to be a more general mechanism for two-component signaling (Silversmith and Bourret, 1999; Stock and Guhaniyogi, 2006; Volkman et al., 2001) and even kinases in general (Buck and Rosen, 2001; Huse and Kuriyan, 2002).

The key subsequent questions are: How is the population shift achieved? How can a protein interconvert among folded substates but avoid unfolding at the same time? What are the molecular pathways for conformational transitions? Here we address these questions by connecting the energetics of functional protein dynamics within the native state to protein folding (Figure 1). Through experimental corroboration of computational prediction (Lei et al., 2009), we infer a molecular pathway for the conformational transition in $NtrC^r$ involving transient hydrogen bonds that stabilize the transition state.

RESULTS AND DISCUSSION

Phosphorylation Acts via Active State Stabilization

Activation of this signaling protein could in principle be achieved by either destabilizing of the inactive state or stabilizing the

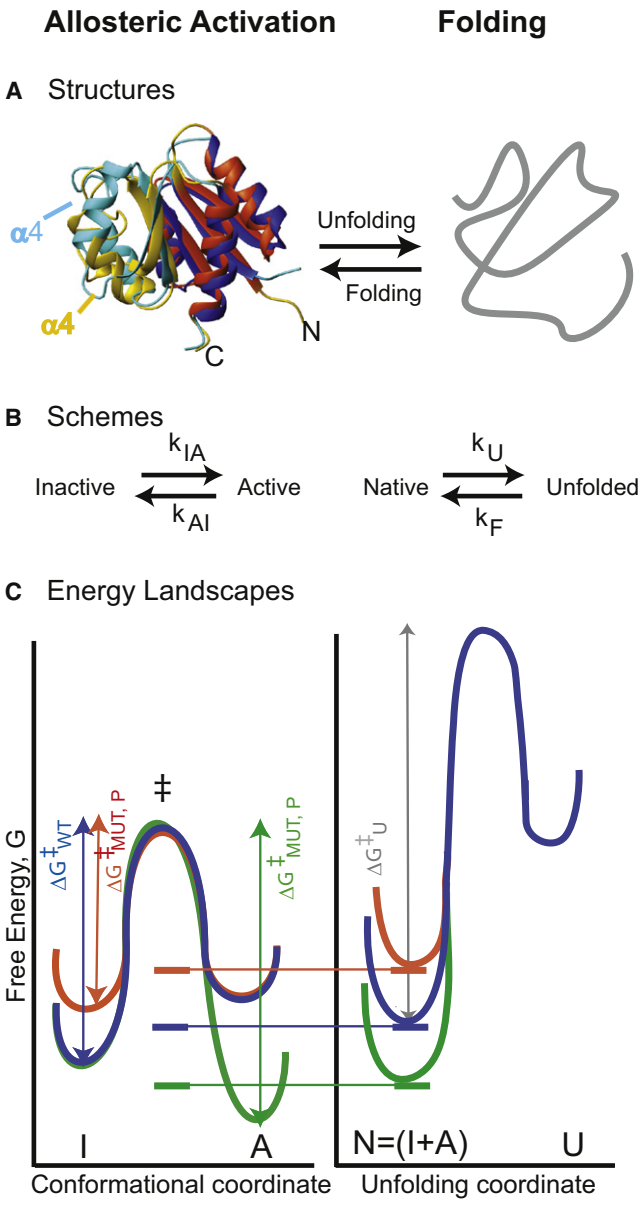

Figure 1. Energetic Relationship between the Energy Landscapes of Activation and Protein Folding of the Signaling Protein NtrC^r

The conformational equilibrium between inactive (I, blue, 1DC7) and active substates (A, orange, 1DC8) in NtrC^r is shown structurally highlighting the switch region in lighter color (A) (modified from Volkman et al., 2001) and schematically (B) with the corresponding rate constants (k_{IA} and k_{AI}).

(C) Theoretical models of a population shift are depicted using a one-dimensional cross-section through the high-dimensional energy landscape for a two-state system in thermal equilibrium. Mutation (MUT) and phosphorylation (P) could shift the equilibrium by an inactive state destabilization (red) and/or active state stabilization (green) relative to wild-type (blue). Discrimination between these mechanisms can be determined through connecting the free-energy changes (horizontal lines) of the native-state ensemble (N = I+A) to the unfolding kinetics, depicted by $\Delta G^{\ddagger}$ and the gray arrow. The free-energy of N is the population-weighted average of the inactive and active states shown as thick horizontal lines.

active one or a combination of both (Figure 1C). These different activation mechanisms can be distinguished by the differences in the microscopic rate constants of the forward and reverse reactions (k_{IA}, k_{AI}, Figure 1B) of the structural transition between the nonphosphorylated inactive wild-type, partially active mutants D86N and D86N/A89T, and phosphomimicking BeF_3^--bound (Hastings et al., 2003), fully active NtrC^r. If mutation or phosphorylation yields a stabilization of the active state, the rate of active to inactive transition would decrease; conversely, a destabilization of the inactive state would result in an increase in the rate of inactive to active transition.

The rate constants were determined using NMR ^{15}N backbone amide CPMG (Carr-Purcell-Meiboom-Gill) relaxation dispersion experiments (Palmer et al., 2001), providing dynamic information for each residue. For residues undergoing micro- to millisecond dynamics, the effective transverse relaxation rate, R_2^{eff}, is increased by an amount R_{ex} in addition to the intrinsic relaxation rate (R_2^0):

$$R_2^{eff}(\nu_{CPMG}) = R_2^0(\nu_{CPMG\to\infty}) + \left(p_I p_A \Delta\omega^2 / k_{ex}\right) \left[1 - (4\nu_{CPMG}/k_{ex})\tanh(k_{ex}/4\nu_{CPMG})\right] \quad (1)$$

(in the limit of fast exchange, kex > > Δω).

The variation of R_{ex} with an applied radio-frequency field (ν_{CPMG}) permits the CPMG dispersion experiment to quantitatively determine kinetics (exchange rate constant, $k_{ex} = k_{IA}+k_{AI}$), thermodynamics (populations p_I and p_A), and structure (chemical shift of exchanging species, $\Delta\omega = \omega_A - \omega_I$) for a two-state exchange process (Loria et al., 1999; Palmer et al., 2001), even for highly skewed populations (Mulder et al., 2001).

Whereas nonphosphorylated and partially activating mutant forms of NtrC^r revealed k_{ex} values faster than 10,000 s^{-1} (Figures 2A–2C), the phosphomimicking species reduced the rate constant of interconversion by an order of magnitude (Figure 2D). From these experiments two qualitative inferences can be drawn. First, for all NtrC^r forms, conformational changes are localized in the previously identified conformational switch region (Kern et al., 1999; Volkman et al., 2001). All such residues can be fit with a single exchange rate constant suggesting that the measured motions correspond to a collective structural transition between the inactive and active substates. Second, an increased exchange rate constant in the mutant forms relative to nonphosphorylated wild-type suggests a population shift by destabilization of the inactive substate. In contrast, the decrease in exchange rate constant for phosphorylated NtrC^r implies a strong stabilization of the active substate upon phosphorylation.

For a quantitative analysis of the energy landscape, the microscopic forward (k_{IA}) and reverse (k_{AI}) rate constants of the structural transition were determined. These rate constants are linked to the equilibrium constant ($K_{eq} = p_A/p_I = k_{IA}/k_{AI}$), which is directly embedded in the population-weighted average resonance position ($\omega_{obs} = p_I \cdot \omega_I + p_A \cdot \omega_A$) for residues undergoing exchange. Consequently, if ω_I and ω_A are known, the equilibrium constant for each form can be directly extracted from its resonance position (Figure 2E). However, the NMR resonance positions of wild-type and BeF_3^--activated NtrC^r are not equivalent to the fully inactive and active substates as both forms exhibit

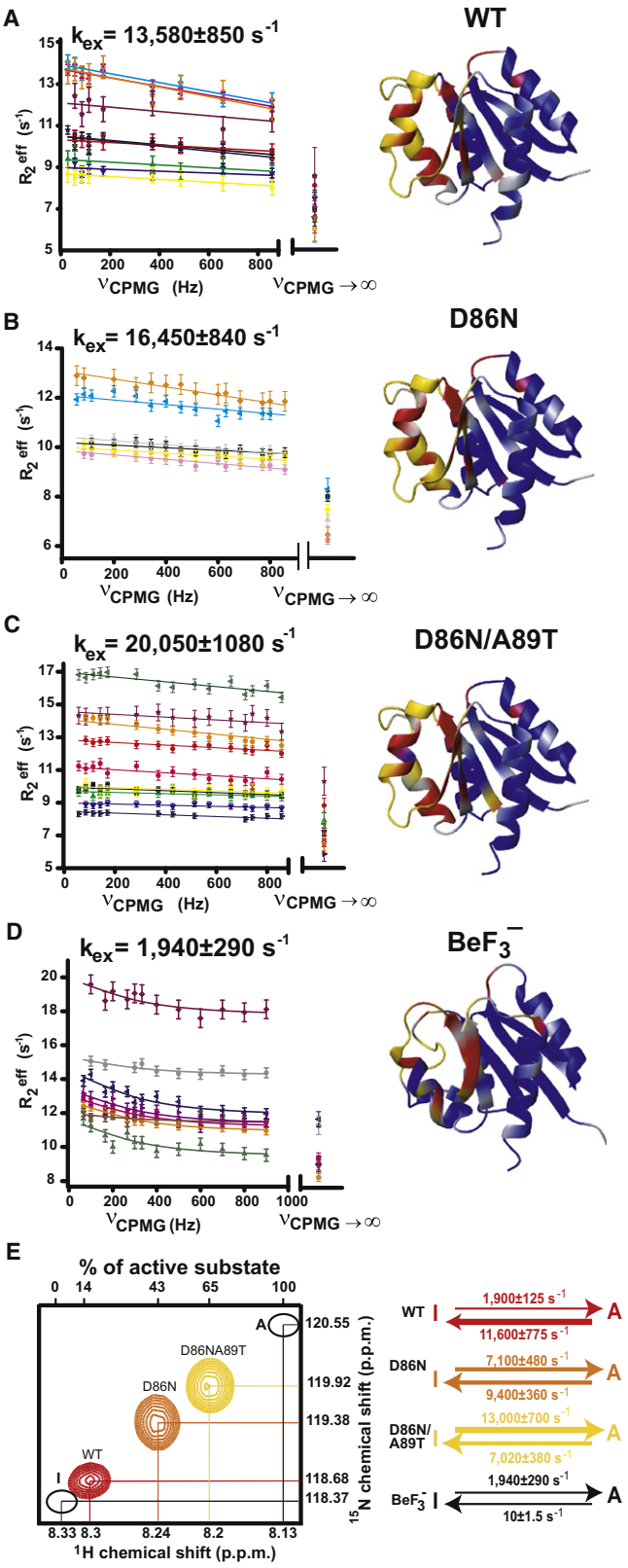

Figure 2. Quantitative Analysis of the Kinetics of the Inactive/Active Conformational Transition

^{15}N CPMG NMR relaxation dispersion data (Palmer, et al., 2001) for wild-type (A), D86N (B), D86N/A89T (C), and BeF_3^--activated NtrC^r at 600 MHz (D) are shown together with the exchange-free transverse relaxation rate ($\nu_{CPMG} \rightarrow \infty$) and the corresponding fitted global exchange rate constants (k_{ex}) as described in Gardino and Kern (2007) and plotted onto the structures of the inactive (A, B, and C) and active (D) structures in red (quantified chemical exchange used for global fitting), yellow (severely exchange broadened), dark blue (no chemical exchange detected), and gray (overlapped/unassigned/proline). The relaxation data for each residue are colored consistently across all four data sets for each functional form of NtrC^r as follows: residue 11 (black), 68 (light pink), 69 (red), 70 (green), 71 (light gray), 72 (blue), 78 (cyan), 82 (magenta), 84 (dark gray), 87 (yellow), 88 (orange), 89 (dark green), 91 (navy blue), 94 (burgundy), 99 (hot pink), 100 (purple), 101 (violet), 102 (royal blue).

(E) The microscopic rate constants (k_{IA} and k_{AI}) were extracted from k_{ex} and the relative populations of the inactive and active states in all NtrC^r forms. The backbone amide resonances of D88 were used as a spectroscopic ruler to determine these populations in conjunction with the dispersion experiments yielding the calculated chemical shifts of fully inactive (I) and active substate (A) (black ovals) (for details see Experimental Procedures). Uncertainties in relaxation rates are the larger of the difference in duplicate points or 2% of the signal to noise ratio. All rates are mean ± standard deviation (SD).

conformational exchange (Figures 2A and 2D). A combined fitting of relaxation dispersion and chemical shift data provided a molecular ruler of the equilibrium for all functional NtrC^r forms and allowed extraction of k_{IA} and k_{AI} (Figure 2E). The results strongly suggest that mutation mainly acts through destabilizing the inactive substate whereas BeF_3^- activation was found to drive the equilibrium almost fully toward the active substate solely by stabilizing the active form as evidenced by an identical k_{IA} rate constant between inactive and active NtrC^r.

Quantitative Validation of the Activation Energy Landscape through the Energetic Correlation to the Folding Energy Landscape

Although these kinetic results indicate an energy landscape in which nonphosphorylated, BeF_3^--activated and the constitutive active mutants of NtrC^r share the same transition state (Figure 5A), a scenario in which the entire energy landscape is shifted along the energy axis for the mutant and/or BeF_3^--activated form relative to wild-type is theoretically possible. This would mean that the mutations and/or BeF_3^- activation would affect both the ground states and the transition state. To address this issue, we depict the reaction coordinate describing the conformational transition within the folded state as energetically connected to a second reaction coordinate describing the folding/unfolding transition (Figures 1C, 5A, and 5B).

Unfolding kinetics for all NtrC^r forms were measured by stopped-flow fluorescence at different guanidinium hydrochloride (GdmHCl) concentrations, and the rate constant of unfolding under native conditions was determined by linear extrapolation to 0 M GdmHCl (Figure 3A) (Fersht, 1999). The unfolding rate constants were found to be about nine orders of magnitude slower than those of the transition within the native state (Figures 2 and 3A). Consequently, for connecting these two energy landscapes through the measured energies, the free energy of the folded form can be treated as a population-weighted average of the inactive and active substates (Figures 1C and 5A). The differences of the activation free energy of unfolding measured

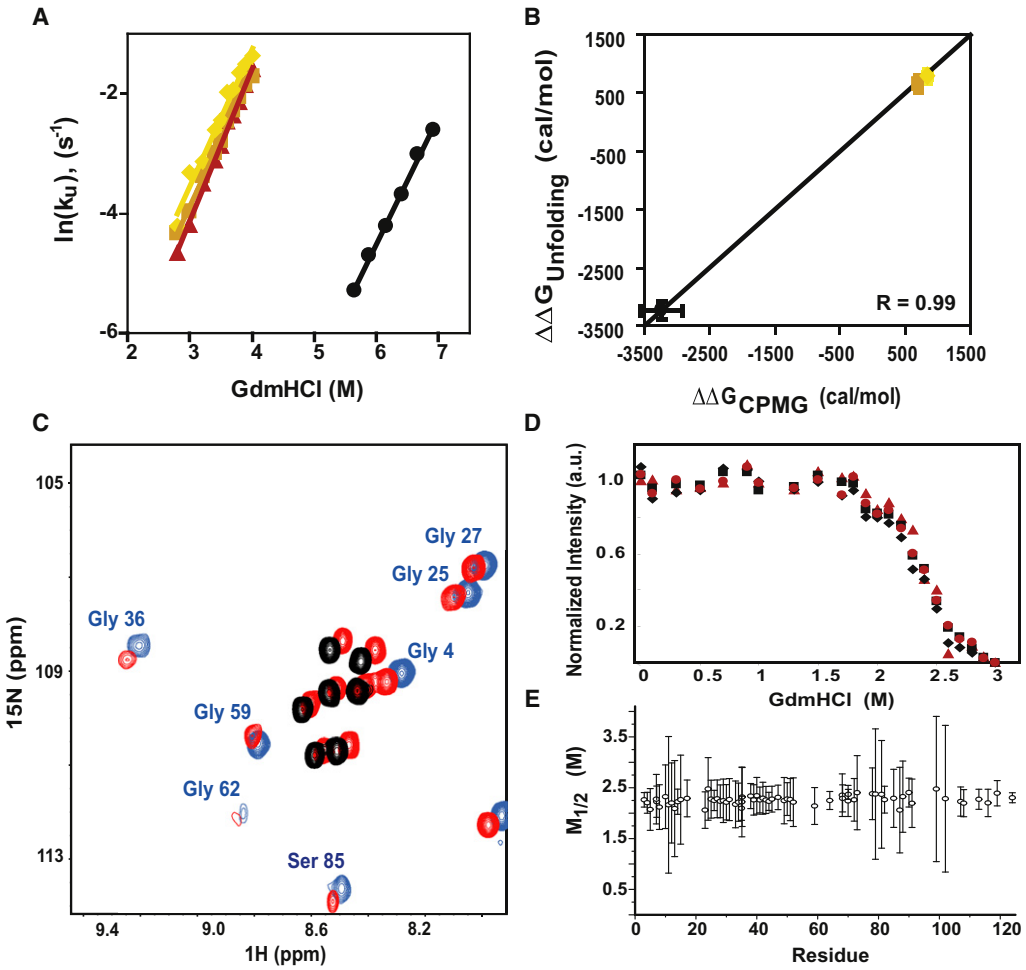

Figure 3. Quantitative Analysis of the Kinetics of the Unfolding/Folding Transition and Its Energetic Correlation to the Activation Kinetics

(A) Kinetics of unfolding (k_u) (mean ± SD) under native conditions were determined for wild-type (red), D86N (orange), D86N/A89T (yellow), and P-NtrC^r (black) by measuring k_u by stopped-flow fluorescence at various guanidinium hydrochloride concentrations and linear extrapolation to 0 M denaturant (Fersht, 1999).

(B) From these unfolding rate constants, differences of the activation free energy of unfolding relative to wild-type ($\Delta\Delta G_{unfolding}$) were calculated (mean ± SD) (see Figure 5) and compared to the corresponding changes in free energy determined from the relaxation dispersion experiments (Figure 2) monitoring the inactive/active substate kinetics ($\Delta\Delta G_{CPMG}$) (mean ± SD), yielding a correlation coefficient of 0.99.

(C) The unfolding/folding transition monitored on a per residue basis by NMR. ^1H ^{15}N HSQC spectra of the folded state (blue with assignments, 1.8 M GdmHCl), the unfolded state (black, 3.2 M GdmHCl), and at denaturant concentrations corresponding to the unfolding transition (red, 2.4 M GdmHCl) are superimposed for the glycine and serine regions of the spectrum. Both the folded and the unfolded peaks are observed at 2.4 M GdmHCl 25°C, the midpoint of unfolding, demonstrating that the unfolding/folding transition is slow on the NMR timescale (less than 10^{-1} s^{-1}) for all residues including helix 4 (Ser85 shown as marker for helix 4).

(D and E) The decreases in intensities of the folded peaks with increasing denaturant concentrations were best fit to a two-state transition. The thermodynamic unfolding curves for all monitored residues including W7 (black diamonds), W17 (black squares), and residues in the alpha 4 helix, T82 (red circles), and D88 (red triangles) are fit to midpoints of transition ($M_{1/2}$) that are within experimental error throughout the protein showing that the entire protein including helix 4 unfolds cooperatively (E). Errors were derived from the rms noise of the individual NMR spectra.

for wild-type, partially active mutants, and phosphorylated NtrC^r quantitatively agree with the corresponding changes in free energy extracted from the inactive/active substate kinetics (Figure 3B). Through a quantitative analysis of two distinct reaction coordinates within the energy landscapes, we were able to validate the energetics underlying the population-shift mechanism (Figures 5A and 5B). We want to highlight the quantitative agreement of the free energy difference for BeF_3^--activated NtrC^r relative to inactive wild-type extracted from the inactive/active transition (Figure 5A) with the one determined from the unfolding kinetics of P-NtrC^r (Figure 5B). This result validates BeF_3^- as a faithful phosphomimic not only in structural terms (Hastings et al., 2003; Kern et al., 1999) but also in respect to the energy landscape of inactive/active interconversion.

The question of the effect of mutations on the ground or transition states has been extensively studied for protein folding, also known as Φ-value analysis (Fersht, 1999; Weikl and Dill, 2007), including the application of NMR relaxation dispersion experiments (Neudecker et al., 2007). In this analysis, changes in the energy landscape through mutations are depicted using

the unfolded state as an energetic reference point. For NtrC^r, the refolding rate constants of all forms are the same; however, the unfolded state as reference point is no longer an assumption but rather a result derived from the connection of the folding landscape to the inactive/active conformational landscape through the measured energies (Figures 5A and 5B).

Pathways of Conformational Transitions Calculated by Molecular Dynamics Simulations

The experiments described above reveal that the functional transitions in NtrC^r occur rapidly whereas the energy barrier for unfolding is much larger. This situation is of course a general requirement for signaling and many other cellular protein functions. The immediate question that emerges is how a protein can rapidly interconvert among folded substates but avoid unfolding at the same time even though many native stabilizing contacts need to be broken during the transition? The answer is embedded in the actual molecular pathways of the conformational transitions. While the structures of the inactive and active substates could be experimentally determined since they represent minima in the energy landscape, structures along the transition pathway cannot be directly monitored in an experiment since they are not significantly populated. However, computational methods can in principle provide high-resolution information of these transition pathways. The challenge lies in current computational sampling times, which are too short relative to the typical microsecond to second conformational transitions in proteins. A variety of pathway methods have been developed to ameliorate this problem for which we cite only a few representative examples (Anthony et al., 2007; Bolhuis, 2008; Christen and van Gunsteren, 2008; Dellago and Bolhuis, 2007; Elber, 2005; Henzler-Wildman and Kern, 2007; Lei et al., 2009; Maragliano et al., 2006; Pan et al., 2008; Rogal and Bolhuis, 2008; Schlitter et al., 1994; Schutkowski et al., 1994; van der Vaart, 2006; Vendruscolo and Dobson, 2005; Yang et al., 2009; for more examples see references therein).

For NtrC^r, transition pathways have been proposed using either coarse-grained models (Latzer et al., 2008; Pan et al., 2008; Vanden-Eijnden and Venturoli, 2009) or all atom simulations suggesting motions in the β3-α3 loop to be crucial for the transition (Hu and Wang, 2006; Khalili and Wales, 2008). Using all atom targeted molecular dynamics simulations (TMD) in explicit water, Lei et al. (2009) predicted a different transition pathway between the active and inactive substates. TMD is a widely used biased molecular simulation method that generates conformational transition pathways through pulling the protein from a starting structure to an end structure via an RMSD (root-mean-square deviation) constraint to the end state (Banavali and Roux, 2005; Israelewitz et al., 2001; Karplus et al., 2005; Ma and Karplus, 1997; Schlitter et al., 1994; van der Vaart, 2006). Briefly, the conformational switch in NtrC^r can be described by a few major stages including a tilt, rotation, and register shift accompanied by a loss and gain of one half helical turn on opposite ends of helix 4 (Figure 1A). Helix 4 is stable during the whole transition. The details of the computational analysis and the predicted pathway have been described (Lei et al., 2009).

The complex nature of this structural rearrangement (Figure 1A) calls for either a pathway with partial unfolding (Latzer et al., 2008) or concerted conformational changes over a large area of the protein (Lei et al., 2009). Using simple native structure-based quadratic potentials, Latzer et al. estimated a barrier height for the activation transition of 54 kcal/mol (Latzer et al., 2008). From this result, they concluded that "protein cracking motions are involved"; i.e., that local unfolding in helix 4 is an essential part of the transition. This high barrier is in contrast to our experimentally determined barrier of only 6 kcal/mol for the activation (Gardino and Kern, 2007) (Figures 2 and 5).

Helix 4 Unfolds Cooperatively with the Remainder of the Protein

Biases and simplifications made in all computational algorithms, including our own simulations using biasing potentials (Lei et al., 2009), require stringent experimental testing. We therefore first measured the stability and rate of unfolding on a per residue basis using NMR (Figure 3). Our fluorescence unfolding experiments determined a 10^9-fold difference in rate constants between the conformational switch and global unfolding (Figures 3 and 5) suggesting that unfolding is not part of the transition pathway. However, the fluorescence experiments do not rule out a transition pathway between the inactive and active conformation through partial unfolding of helix 4 particularly because the fluorescence markers Trp7 and Trp17 are not located in the conformational switch region. Using NMR, helix 4 was found to have the same stability as the remainder of the protein (Figures 3C–3E) and the NMR stability data agree with the fluorescence data (Figure 3E and Figure S5 available online). Moreover, the rate constant of unfolding of residues in helix 4 is at least five orders of magnitude slower (Figure 3C) than the conformational switch within the native state. We note that the performed stopped-flow fluorescence and NMR unfolding experiments were not intended to unravel the detailed pathway of unfolding, a question extensively studied for many proteins in the last decades, but rather aimed to energetically evaluate the native-state energy landscape including the predicted activation pathway. The NMR unfolding results rule out a pathway with partial unfolding (Latzer et al., 2008) and are qualitatively consistent with the computed pathway comprised of multistep concerted rearrangements (Lei et al., 2009).

"Non-native" Hydrogen Bonds Lower the Activation Barrier

We then thought to test the computationally predicted transition pathway (Lei et al., 2009) experimentally by identifying atomic interactions that might stabilize this pathway. We particularly sought energetically correlated events in the TMD trajectories. The TMD simulations forward the idea that breakage of two backbone hydrogen bonds at the C-terminal end of helix 4, resulting in a loss of half of a helical turn, seem to be energetically compensated for by formation of a few transient hydrogen bonds. Those include hydrogen bonds between the side chains of S85 and D86 at the top of helix 4 and between the side chains of Q96 and Y101 connecting the bottom of helix 4 and strand 5 (Figure 4A; Lei et al., 2009). These non-native hydrogen bonds are present only during the transition but not in the active or inactive states. Two new main chain hydrogen bonds are then

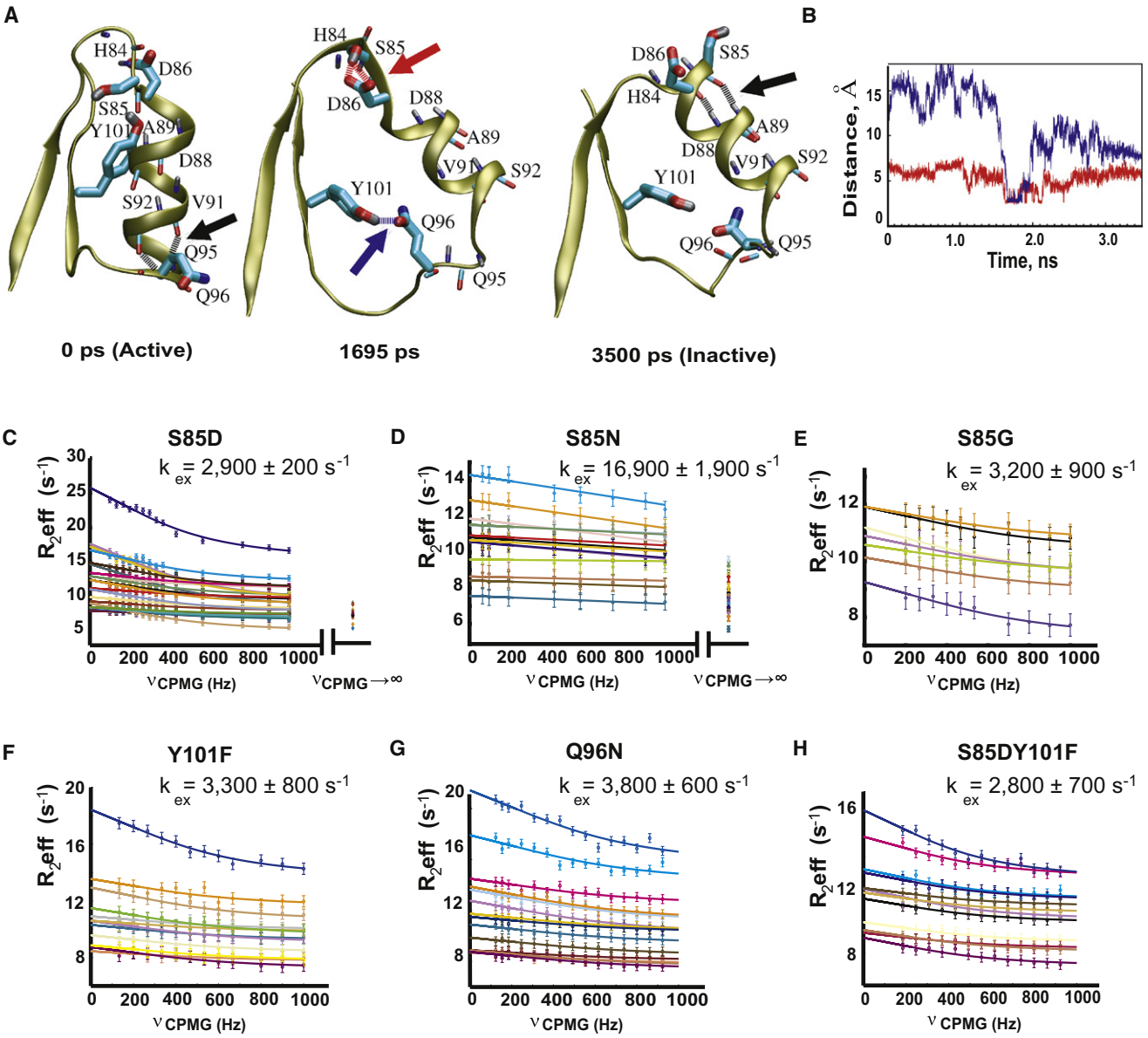

Figure 4. Experimental Identification of the Transition Landscape for Activation

(A) Prediction of two transient non-native hydrogen bonds that lower the energy of the transition landscape using TMD (Lei et al., 2009). Snapshots of the active (starting point of TMD), inactive state (end point of TMD), and during the transition (1695 ps) are shown. In the active state, the C-terminal residues of helix 4, Q96 and Q95, are shown with their corresponding helical backbone hydrogen bonds (black arrow). In the inactive state, these hydrogen bonds are replaced by two new helical hydrogen bonds for S85 and H84 (black arrow) resulting in the register shift of helix 4. During the transition (middle panel), side-chain hydrogen bonds are formed between S85 and D86 (red arrow) and between Y101 and Q96 (blue arrow).

(B) Corresponding time trace of the distance between the hydroxyl hydrogen of S85 and the carboxylate oxygens of D86 (red) and Y101 and Q96 (blue) in the simulation (Lei et al., 2009). Experimental testing of this transition landscape through removal (C and E) and restoration (D) of the S85-D86 transient hydrogen bond and removal (F and G) of the Y101-Q96 hydrogen bond or the combination of both (H). For all mutant forms, the transition rate constants (k_{ex}) were measured using ^{15}N NMR relaxation dispersion experiments. The dispersion curves are color coded as follows: residues 5 (peach), 6 (ivory), 9 (raspberry), 10 (burnt sienna), 11 (black), 12 (slate), 16 (rose), 18 (maroon), 29 (salmon), 30 (plum), 35 (lavender), 36 (orange-yellow), 47 (teal), 49 (sage), 50 (mustard), 64 (brown), 68 (light pink), 69 (red), 71 (light gray), 78 (cyan), 79 (light blue), 81 (lime), 82 (magenta), 83 (periwinkle), 87 (yellow), 88 (orange), 90 (light brown), 91 (navy blue), 102 (royal blue), 106 (sea green), 119 (jade), 122 (dark brown). Uncertainties in relaxation rates are the larger of the difference in duplicate points or 2% of the signal to noise ratio. All rates are mean ± SD.

formed between H84 and D88 and between S85 and A89 adding a half helical turn to complete the helical register shift and thereby the transition to the inactive state (Figure 4A).

To test the validity of this network of correlated motions during the transition, we disrupted these putative transient hydrogen bonds by mutagenesis (Figure 4). Strikingly, replacing S85 with

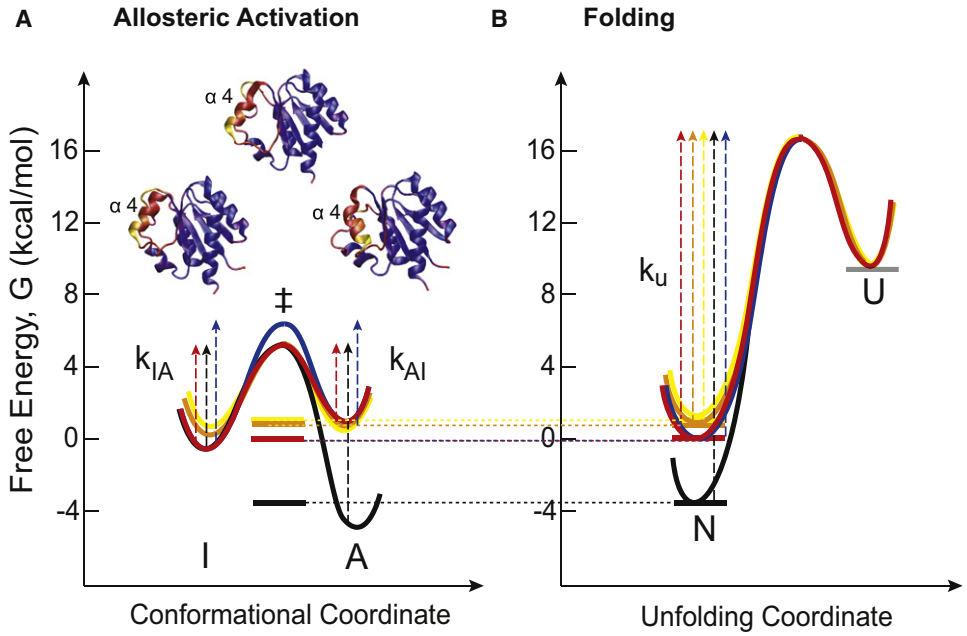

Figure 5. Mechanism of Activation and Molecular Transition Pathway Rationalizing Fast Signaling without Unfolding

Quantitative description of the energy landscape of activation of $NtrC^r$ (A) and its energetic relation to unfolding (B). Mechanism of the equilibrium shift between the inactive and active states through mutation (D86N orange, D86N/A89T yellow) or BeF_3^- activation (black) relative to wild-type (red, G of inactive wild-type was arbitrarily set to 0) was characterized using NMR CPMG relaxation dispersion (Figures 2A–2D) (A) and validated through the corresponding unfolding rate constants, k_u (B), that quantitatively match the free-energy changes calculated from the NMR relaxation experiments (indicated by dotted horizontal lines connecting the population average free energy of the inactive and active states, I + A, to the unfolding energy landscape). The activation free energies, calculated from the corresponding measured rate constants, k_{IA}, k_{AI}, and k_u, are shown for all $NtrC^r$ forms as dashed vertical arrows using the matching colors. The free energy of the transition landscape (‡) was increased through the removal of the transient side chain S85-D86 hydrogen bond on the top of helix 4 or Y101-Q96 hydrogen bond at the bottom of helix 4 (blue) supporting the calculated transition pathway from TMD (Lei et al., 2009). The structures of the inactive (1DC7) and active (1DC8) states and a snapshot from the TMD trajectory representing the transition region are shown highlighting the switch region by a color scale from blue to red to yellow with increasing root-mean-square deviation relative to the starting active conformation.

an aspartate resulted in a decrease in the rate constant of inactive/active interconversion from about 14,000 s^{-1} for wild-type to about 3,000 s^{-1} for this S85D mutant (Figure 4C). Moreover, a mutation that restores the hydrogen bond donor capacity at position 85 (S85N) restores the fast interconversion rate of wild-type (Figure 4D). The decrease in rate in S85D is not due to the introduction of a charge since S85G produces the same slow rate as S85D (Figure 4E). Importantly, the spectra of S85D, S85G, and S85N are almost identical to the wild-type spectrum (Figure S6). These data indicate that neither the structures nor the relative populations of the inactive and active states are altered. This result is further buttressed by 20 ns MD simulations of both mutant forms in the inactive and active states (Figure S7). Furthermore, we set out to follow up the experimental data on the NtrC mutant forms with disrupted transient hydrogen bonds by new TMD simulations on these mutants. We find that both mutant forms reveal the same transition stages as the TMD simulation on the wild-type protein, but without the transient non-native hydrogen bonds between S85 and D86.

We infer that the transient hydrogen bond between S85 and D86 lowers the activation barrier of the slowest step in the overall conformational transition by about 1 kcal/mol. Finally, the identical unfolding rates for wild-type and S85D complete the quantitative description of the energy landscapes by identifying this hydrogen bond as affecting only the free energy of the transition state (Figures 5 and S6).

The concept that non-native hydrogen bonds reduce the barrier for this complex conformational transition is buttressed by additional experiments that disrupt the hydrogen bond between Q96 and Y101. Both Y101F and Q96N mutations significantly decrease the interconversion rate constant (Figures 4F and 4G). The reduction of the interconversion rate constant by shortening the side chain of the hydrogen bond acceptor (Q96N mutation) reveals that in addition to the presence of the hydrogen bond acceptor/donor pair, a quite specific distance between them is required.

Removal of both transient hydrogen bonds does not further decrease the interconversion rate constant (Figure 4H), suggesting that they influence the free energy of the system at slightly different parts of the transition pathway. These experimental results further demonstrate the complex multidimensional nature of the transition energy landscape. We note that the described experiments do not allow characterization of the entire complex pathway; however, they provide critical information about structural configurations that are not only along the pathway but also influence the energy of the transition states. Thus these configurations serve as key starting points for further extensive unbiased computational exploration of the multidimensional energy

landscape, which is beyond our current scope and in fact beyond current methodology. We feel that direct experimental testing of computational predictions, which is done in this work, is the strongest validation of simulations.

Conclusions

The concept of preexisting equilibria within the folded state and their roles in biological function such as enzyme catalysis, signaling, and ligand binding has become widely accepted (Monod et al., 1965; Boehr et al., 2006a, 2006b; Frauenfelder et al., 1991; Henzler-Wildman and Kern, 2007; Henzler-Wildman et al., 2007; Kumar et al., 2000; Li et al., 2008; Silversmith and Bourret, 1999; Stock and Guhaniyogi, 2006; Volkman et al., 2001; Lau and Roux, 2007; Ravindranathan et al., 2005; Yang et al., 2009). We now show that rare excursions to the active conformation are essential for activating the NtrC protein since the data suggest that only the higher-energy active conformation can be phosphorylated. This conclusion is supported structurally by the solvent inaccessibility of D54, the site of phosphorylation, in the inactive conformation. Although our earlier work indicated that activation is mediated via a shift in preexisting populations, we have now characterized the underlying molecular mechanism. Selective binding to a minimally populated conformation that is usually "hidden" to traditional structural methods may be a general mechanism for other kinases (Buck and Rosen, 2001; Huse and Kuriyan, 2002) or may be more general for ligand binding (Henzler-Wildman and Kern, 2007; Li et al., 2008).

Overall our findings shed light into possible mechanisms of *how* proteins can efficiently change conformations that require complicated realignment of multiple atomic contacts while avoiding unfolding. The marriage between experiment and computation has provided a glimpse into molecular pathways of interconversion, thereby expanding the energy landscape from the ground states to "transition landscapes." The signaling domain $NtrC^r$ has apparently solved the problem of stability in the face of loss of native stabilizing contacts during activation through fine-tuned concerted motions. These motions result in a roughly "isoenergetic" transition involving non-native transient atomic interactions that are used to "hold on" to the free energy until the final new native contacts of the active state are built, thereby circumventing the risk of unwanted unfolding during the transition. Our results on $NtrC^r$ illustrate sophisticated "designer" principles in proteins through the multifaceted use of specific atoms that guarantee not only one stable folded structure but also efficient interconversion among functionally essential ensembles of structures. The list of transient atomic interactions for $NtrC^r$ is currently incomplete; however, the concept of non-native interactions lowering the energy barrier may help to improve the current limited success in the design of protein function, such as enzyme catalysis, drug binding, and protein-protein interactions.

EXPERIMENTAL PROCEDURES

Sample Preparation

Unlabeled and uniformly ^{15}N-labeled $NtrC^r$ wild-type, mutant forms, phosphorylated, and BeF_3^--activated $NtrC^r$ were prepared as previously described (Hastings et al., 2003; Volkman et al., 2001). All NMR samples were 0.75 mM $NtrC^r$ in 50 mM NaP buffer, pH 6.75, with 10% D_20.

NMR Experiments

TROSY ^{15}N CPMG relaxation dispersion experiments (Loria et al., 1999; Mulder et al., 2001; Palmer et al., 2001; Tollinger et al., 2001) were acquired on a Varian Inova 600 and a Bruker Avance 800 spectrometer equipped with a cryoprobe at 298K with constant time T_2 delays between 60 and 70 ms, which roughly yielded 55% of residual signal intensity, and CPMG field strengths between 28 and 1000 Hz. The data were fit as described (Henzler-Wildman et al., 2007). The method to determine the exchange-free transverse relaxation time (R_2^0, $\nu_{CPMG} \rightarrow \infty$) and its usage in the global fits of the relaxation dispersion data are described (Gardino and Kern, 2007). ^{15}N R_1 values were measured using standard experiments (Farrow et al., 1994). R_1^H values were measured using a TROSY-based R_1^{HzNz} pulse sequence employing a REBURP pulse to selectively invert the amide region (Gardino and Kern, 2007). Data were processed using NMRPipe (Delaglio et al., 1995). Intensities were fit to a mono-exponential decay curve, and uncertainties were measured from duplicate points and an estimate of signal-to-noise (2% of R_2^{eff}).

Determination of Populations

Final active state populations (p_A) for each functional form of $NtrC^r$ were determined through the following equation:

$$p_A = \left(\delta^{exp} - \delta^{I,calc}\right) / \delta^{\Delta\omega,calc}$$

where δ^{exp} is the experimental chemical shift value in the indirect dimension (^{15}N) taken from a 2D ^1H-^{15}N correlated HSQC NMR spectrum, $\delta^{I,calc}$ is the calculated endpoint representing the fully inactive chemical shift value, and $\delta^{\Delta\omega,calc}$ is the calculated difference in chemical shift between the inactive ($\delta^{I,calc}$) and active ($\delta^{A,calc}$) state endpoints. Whereas δ^{exp} can be directly read out from the HSQC spectra (Figure 2E), $\delta^{I,calc}$ and $\delta^{A,calc}$ are not known since the chemical shifts of both wild-type and BeF_3^--activated forms do not represent the true endpoints. The difference in chemical shift between wild-type and BeF_3^--activated $NtrC^r$, however, provided a lower limit of $\Delta\omega$. Only extremely skewed populations of BeF_3^- $NtrC^r$ ($p_A \geq 0.994$) yielded chemical shift differences ($\Delta\omega$) on a per residue basis that were large enough to fit the experimentally observed displacements. Incorporation of CPMG dispersion of wild-type, BeF_3^--activated, D86N, and D86NA89T $NtrC^r$ together with the corresponding chemical shift changes (Figure 2E), which also emulated their respective activities (Volkman et al., 2001), then allowed us to estimate the relative populations of active and inactive states for each $NtrC^r$ form (see Table S1). A good correlation was found between the experimentally observed amide backbone chemical shift position for D88 and other residues with the calculated populations computed for the wild-type and mutant forms of $NtrC^r$. In addition, $\Delta\omega$ values fitted from the CPMG dispersion showed good agreement among different $NtrC^r$ forms for residues that are not locally perturbed in chemical shift due to the proximity of either BeF_3^- or mutation (see Table S1). For the BeF_3^--activated form and the transition-state mutant forms (S85D and Y101F), global fitting of the CPMG data collected at 600 MHz and 800 MHz was possible because the exchange in these proteins is in the time regime in which R_{ex} can be sufficiently suppressed with the imparted ν_{CPMG} field strength. Global fitting data from two external magnetic field strengths further confirmed the exchange rate constants and populations (Figure S1).

Folding and Unfolding Kinetics

Unfolding kinetics were measured at 298K by stopped-flow fluorescence or discontinuously for P-$NtrC^r$ by mixing protein stock solution with GdmCl in a 1:1 ratio to a final concentration of $\geq$3.2M denaturant and 5 μM protein. The sample was excited at 281 nm and emission measured using a 320 nm long-pass filter. Sequential stopped-flow was used to measure the rate constants of folding in order to overcome the slow phase due to cis/trans prolyl isomerization (Figure S2). 250 μM $NtrC^r$ was mixed 1:1 with denaturant to a final concentration $\geq$3.2M for 10 s followed by a 1:1 mixing with buffer yielding a final denaturant concentration between 1.6–2.0 M and a 62.5 μM final protein concentration. An average of 10 (unfolding) and 30 (folding) scans were best fit to single exponentials.

Unfolding of wild-type $NtrC^r$ by NMR at 298K was measured by ^{15}N-HSQC's at various GdmCl concentrations and the decrease in the peak intensities of the folded form, corrected for the effect of ionic strength on the peak intensity,

were fit to a sigmoidal curve to determine the stability of each residue (Figures S3–S5).

Conversion of Rate Constants to Energy

For visualization of the experimentally determined kinetic and thermodynamic values in form of an energy landscape, changes in free energies were calculated from the ratio of the rate constants. The differences in free energies between the inactive and active substates for wild-type were calculated according to $\Delta G = -RT\ln(k^{IA}/k^{AI})$. Changes of the free energies of mutant forms and BeF_3^--activated NtrC^r relative to wild-type were then determined from the changes in the microscopic rate constants of the interconversion process (k_{IA}, k_{AI}) using the following equation according to standard transition state theory assuming an identical pre-exponential factor for the wild-type and mutant forms:

$\Delta\Delta G^{\ddagger,IA}_{CPMG} = -RT\ln(k^{IA,wild\text{-}type}/k^{IA,mutant,BeF_3^-})$ and $\Delta\Delta G^{\ddagger,AI}_{CPMG} = -RT\ln(k^{AI,wild\text{-}type}/k^{AI,mutant,BeF_3^-})$ where R is the universal gas constant.

We then set the population-weighted average of the free energy of wild-type to zero. Changes in the free energies of the native state of the mutant forms relative to wild-type could then be determined by comparing the population-averaged free energies ($\Delta\Delta G_{CPMG}$).

The energy landscape derived from these calculations was quantitatively verified by determining the changes in unfolding rate constants that consequently reflect the changes in the free energies of the folded states. The same equations were used to determine the differences in the free energies of unfolding: $\Delta\Delta G^{\ddagger}_{unfolding} = -RT\ln(k_u^{wild\text{-}type}/k_u^{mutant,BeF3^-})$. We note that the absolute values of $\Delta G^{\ddagger\ IA}$ and $\Delta G^{\ddagger}_{unfolding}$ depend on the pre-exponential factor for which we used a value described in the literature for protein folding ($10^6\ s^{-1}$) (Kubelka et al., 2004). However, for the important comparison of energy changes between different forms of NtrC^r ($\Delta\Delta G$), it is reasonable to assume very similar pre-exponential factors among the NtrC^r forms for each separate process, in which case they are canceling out as assumed in the equation above. The strong agreement of the $\Delta\Delta G$ values determined from the inactive/active transition within the folded state and the $\Delta\Delta G$ values determined from unfolding validates this assumption.

Computation

MD and TMD simulations were performed in explicit solvent, with TIP3P water molecules (Price and Brooks, 2004), using the simulation program CHARMM (Brooks et al., 1983) version c31b1 with the all atom force field C22 (MacKerell et al., 1998) and the CMAP correction for the protein backbone dynamics (MacKerrell et al., 2004) as described in Lei et al. (2009).

SUPPLEMENTAL DATA

Supplemental Data include eight figures and two tables and can be found with this article online at http://www.cell.com/supplemental/S0092-8674(09)01434-2.

ACKNOWLEDGMENTS

We thank Dr. Martin Karplus for a fruitful collaboration and helpful discussions in the computational studies that led to the predicted pathway, Dr. Chunyu Wang at Columbia University for providing us with a pulse sequence to measure R_{ex} in large proteins and for helpful discussions, Dr. Lewis E. Kay at the University of Toronto for the R_1^{HzNz} pulse sequence, and Dr. Jack Skalicky at the NHMFL at Florida with support from NSF for NMR time. This work was supported by the Howard Hughes Medical Institute, NIH grants to D.K. (GM62117 and GM67963), a DOE grant (Office of Basic Energy Sciences) to D.K (DE-FG02-05ER15699), and instrumentation grants by the NSF and the Keck foundation to D.K.

Received: May 26, 2009
Revised: August 3, 2009
Accepted: November 4, 2009
Published: December 10, 2009

REFERENCES

Anthony, M.A.W., Ron, E., and David, S. (2007). Extending molecular dynamics time scales with milestoning: Example of complex kinetics in a solvated peptide. J. Chem. Phys. *126*, 145104.

Austin, R.H., Beeson, K.W., Eisenstein, L., Frauenfelder, H., and Gunsalus, I.C. (1975). Dynamics of ligand binding to myoglobin. Biochemistry *14*, 5355–5373.

Banavali, N.K., and Roux, B. (2005). The N-terminal end of the catalytic domain of Src kinase Hck is a conformational switch implicated in long-range allosteric regulation. Structure *13*, 1715–1723.

Boehr, D.D., Dyson, H.J., and Wright, P.E. (2006a). An NMR perspective on enzyme dynamics. Chem. Rev. *106*, 3055–3079.

Boehr, D.D., McElheny, D., Dyson, H.J., and Wright, P.E. (2006b). The dynamic energy landscape of dihydrofolate reductase catalysis. Science *313*, 1638–1642.

Bolhuis, P.G. (2008). Rare events via multiple reaction channels sampled by path replica exchange. J. Chem. Physiol. *129*, 114108.

Brooks, B.R., Bruccoleri, R.E., Olafson, B.D., States, D.J., Swaminathan, S., and Karplus, M. (1983). CHARMM- a program for macromolecular energy, minimization, and dynamics calculations. J. Comput. Chem. *4*, 187–217.

Buck, M., and Rosen, M.K. (2001). Structural biology. Flipping a switch. Science *291*, 2329–2330.

Christen, M., and van Gunsteren, W.F. (2008). On searching in, sampling of, and dynamically moving through conformational space of biomolecular systems: A review. J. Comput. Chem. *29*, 157–166.

Delaglio, F., Grzesiek, S., Vuister, G.W., Zhu, G., Pfeifer, J., and Bax, A. (1995). NMRPipe - a multidimensional spectral processing system based on Unix pipes. J. Biomol. NMR *6*, 277–293.

Dellago, C., and Bolhuis, P.G. (2007). Transition path sampling simulations of biological systems. In Atomistic Approaches in Modern Biology: From Quantum Chemistry to Molecular Simulations (New York: Springer), pp. 291–317.

Dill, K.A., and Chan, H.S. (1997). From levinthal to pathways to funnels. Nat. Struct. Biol. *4*, 10–19.

Dobson, C.M., Sali, A., and Karplus, M. (1998). Protein folding: A perspective from theory and experiment. Angew. Chem. Int. Ed. *37*, 868–893.

Elber, R. (2005). Long-timescale simulation methods. Curr. Opin. Struct. Biol. *15*, 151–156.

Farrow, N.A., Muhandiram, R., Singer, A.U., Pascal, S.M., Kay, C.M., Gish, G., Shoelson, S.E., Pawson, T., Forman-Kay, J.D., and Kay, L.E. (1994). Backbone dynamics of a free and phosphopeptide-complexed Src homology 2 domain studied by 15N NMR relaxation. Biochemistry *33*, 5984–6003.

Fersht, A. (1999). Structure and Mechanism in Protein Science: A Guide to Enzyme Catalysis and Protein Folding (New York: W.H. Freeman and Company).

Frauenfelder, H., Sligar, S.G., and Wolynes, P.G. (1991). The energy landscapes and motions of proteins. Science *254*, 1598–1603.

Gardino, A.K., and Kern, D. (2007). Functional dynamics of response regulators using NMR relaxation techniques. Methods Enzymol. *423*, 149–165.

Hastings, C.A., Lee, S.Y., Cho, H.S., Yan, D., Kustu, S., and Wemmer, D.E. (2003). High-resolution solution structure of the beryllofluoride-activated NtrC receiver domain. Biochemistry *42*, 9081–9090.

Henzler-Wildman, K., and Kern, D. (2007). Dynamic personalities of proteins. Nature *450*, 964–972.

Henzler-Wildman, K.A., Thai, V., Lei, M., Ott, M., Wolf-Watz, M., Fenn, T., Pozharski, E., Wilson, M.A., Petsko, G.A., Karplus, M., et al. (2007). Intrinsic motions along an enzymatic reaction trajectory. Nature *450*, 838–844.

Hu, X., and Wang, Y. (2006). Molecular dynamic simulations of the N-terminal receiver domain of NtrC reveal intrinsic conformational flexibility in the inactive state. J. Biomol. Struct. Dyn. *23*, 509–518.

Huse, M., and Kuriyan, J. (2002). The conformational plasticity of protein kinases. Cell *109*, 275–282.

Israelewitz, B., Gao, M., and Schulten, K. (2001). Steered molecular dynamics and mechanical functions of proteins. Curr. Opin. Struct. Biol. *11*, 224–230.

Karplus, M., Gao, Y.Q., Ma, J., van der Vaart, A., and Yang, W. (2005). Protein structural transitions and their functional role. Philos. Transact. A Math. Phys. Eng. Sci. *363*, 331–355.

Kern, D., Volkman, B.F., Luginbuhl, P., Nohaile, M.J., Kustu, S., and Wemmer, D.E. (1999). Structure of a transiently phosphorylated switch in bacterial signal transduction. Nature *402*, 894–898.

Khalili, M., and Wales, D.J. (2008). Pathways for conformational change in nitrogen regulatory protein C from discrete path sampling. J. Phys. Chem. B *112*, 2456–2465.

Kubelka, J., Hofrichter, J., and Eaton, W.A. (2004). The protein folding 'speed limit'. Curr. Opin. Struct. Biol. *14*, 76–88.

Kumar, S., Ma, B., Tsai, C.J., Sinha, N., and Nussinov, R. (2000). Folding and binding cascades: dynamic landscapes and population shifts. Protein Sci. *9*, 10–19.

Latzer, J., Shen, T., and Wolynes, P.G. (2008). Conformational switching upon phosphorylation: a predictive framework based on energy landscape principles. Biochemistry *47*, 2110–2122.

Lau, A.Y., and Roux, B. (2007). The free energy landscapes governing conformational changes in a glutamate receptor ligand-binding domain. Structure *15*, 1203–1214.

Lei, M., Velos, J., Gardino, A., Kivenson, A., Karplus, M., and Kern, D. (2009). Segmented transition pathway of the signaling protein nitrogen regulatory protein C. J. Mol. Biol. *392*, 823–836.

Li, P., Martins, I.R., Amarasinghe, G.K., and Rosen, M.K. (2008). Internal dynamics control activation and activity of the autoinhibited Vav DH domain. Nat. Struct. Mol. Biol. *15*, 613–618.

Loria, J.P., Rance, M., and Palmer, A.G. (1999). A relaxation-compensated Carr-Purcell-Meiboom-Gill sequence for characterizing chemical exchange by NMR spectroscopy. J. Am. Chem. Soc. *121*, 2331–2332.

Ma, J., and Karplus, M. (1997). Molecular switch in signal transduction: reaction paths of the conformational changes in ras p21. Proc. Natl. Acad. Sci. USA *94*, 11905–11910.

MacKerell, J.A.D., Bashford, D., Bellott, M., Dunbrack, R.L., Jr., Evanseck, J.D., Field, M.J., Fischer, S., Gao, J., Guo, H., Ha, S., et al. (1998). All-atom empirical potential for molecular modeling and dynamics studies of proteins. J. Phys. Chem. *102*, 3586–3616.

MacKerrell, A.D., Feig, M., and Brooks, C.L., III. (2004). Extending the treatment of backbone energetics in protein force fields: Limitations of gas-phase quantum mechanics in reproducing protein conformational distributions in molecular dynamics simulations. J. Comput. Chem. *25*, 1400–1415.

Maragliano, L., Fischer, A., Vanden-Eijnden, E., and Ciccotti, G. (2006). String method in collective variables: Minimum free energy paths and isocommittor surfaces. J. Chem. Physiol. *125*, 24106.

Monod, J., Wyman, J., and Changeux, J.P. (1965). On the nature of allosteric transitions: A plausible model. J. Mol. Biol. *12*, 88–118.

Mulder, F.A., Mittermaier, A., Hon, B., Dahlquist, F.W., and Kay, L.E. (2001). Studying excited states of proteins by NMR spectroscopy. Nat. Struct. Biol. *8*, 932–935.

Neudecker, P., Zarrine-Afsar, A., Davidson, A.R., and Kay, L.E. (2007). Phi-value analysis of a three-state protein folding pathway by NMR relaxation dispersion spectroscopy. Proc. Natl. Acad. Sci. USA *104*, 15717–15722.

Palmer, A.G., 3rd, Kroenke, C.D., and Loria, J.P. (2001). Nuclear magnetic resonance methods for quantifying microsecond-to-millisecond motions in biological macromolecules. Methods Enzymol. *339*, 204–238.

Pan, A.C., Sezer, D., and Roux, B. (2008). Finding transition pathways using the string method with swarms of trajectories. J. Phys. Chem. B *112*, 3432–3440.

Price, D.J., and Brooks, C.L., III. (2004). A modified TIP3P water potential for simulation with Ewald summation. J. Chem. Physiol. *121*, 10096–10103.

Ravindranathan, K.P., Gallicchio, E., and Levy, R.M. (2005). Conformational equilibria and free energy profiles for the allosteric transition of the ribose-binding protein. J. Mol. Biol. *353*, 196–210.

Rogal, J., and Bolhuis, P.G. (2008). Multiple state transition path sampling. J. Chem. Physiol. *129*, 224107.

Schlitter, J., Engels, M., and Kruger, P. (1994). Targeted molecular dynamics: a new approach for searching pathways of conformational transitions. J. Mol. Graph. *12*, 84–89.

Schutkowski, M., Neubert, K., and Fischer, G. (1994). Influence on proline-specific enzymes of a substrate containing the thioxoaminoacyl-prolyl peptide bond. Eur. J. Biochem. *221*, 455–461.

Silversmith, R.E., and Bourret, R.B. (1999). Throwing the switch in bacterial chemotaxis. Trends Microbiol. *7*, 16–22.

Stock, A.M., and Guhaniyogi, J. (2006). A new perspective on response regulator activation. J. Bacteriol. *188*, 7328–7330.

Stock, A.M., Robinson, V.L., and Goudreau, P.N. (2000). Two-component signal transduction. Annu. Rev. Biochem. *69*, 183–215.

Tollinger, M., Skrynnikov, N.R., Mulder, F.A.A., Forman-Kay, J.D., and Kay, L.E. (2001). Slow dynamics in folded and unfolded states of an SH3 domain. J. Am. Chem. Soc. *123*, 11341–11352.

Tsai, C.J., Del Sol, A., and Nussinov, R. (2009). Protein allostery, signal transmission and dynamics: a classification scheme of allosteric mechanisms. Mol. Biosyst. *5*, 207–216.

van der Vaart, A. (2006). Simulation of conformational transitions. Theor. Chem. Acc. *116*, 183–193.

Vanden-Eijnden, E., and Venturoli, M. (2009). Revisiting the finite temperature string method for the calculation of reaction tubes and free energies. J. Chem. Phys. *130*, 194103.

Vendruscolo, M., and Dobson, C.M. (2005). Towards complete descriptions of the free-energy landscapes of proteins. Philos. Transact. A Math. Phys. Eng. Sci. *363*, 433–450.

Volkman, B.F., Lipson, D., Wemmer, D.E., and Kern, D. (2001). Two-state allosteric behavior in a single-domain signaling protein. Science *291*, 2429–2433.

Weikl, T.R., and Dill, K.A. (2007). Transition-states in protein folding kinetics: the structural interpretation of Phi values. J. Mol. Biol. *365*, 1578–1586.

Wolynes, P.G. (2005). Recent successes of the energy landscape theory of protein folding and function. Q. Rev. Biophys. *38*, 405–410.

Yang, S., Banavali, N.K., and Roux, B. (2009). Mapping the conformational transition in Src activation by cumulating the information from multiple molecular dynamics trajectories. Proc. Natl. Acad. Sci. USA *106*, 3776–3781.